BIBECHANA
Vol. 22, No. 1, April 2025, 63-72

ISSN 2091-0762 (Print), 2382-5340 (Online)
Journal homepage: http://nepjol.info/index.php/BIBECHANA
Publisher:Dept. of Phys., Mahendra Morang A. M. Campus (Tribhuvan University)Biratnagar

Thermal properties and non-bonded interactions in human PMP2 variants: A molecular dynamics study

Prabin Aryal, Jhulan Powrel

Department of Physics, Butwal Multiple Campus, Tribhuvan University
*Corresponding author. Email: prabinaryal.0d@gmail.com(PA)
jhulan.sumi@gmail.com(JP)

Abstract

Charcot-Marie-Tooth disease, a genetic disorder linked to mutations in the peripheral myelin protein 2, currently lacks an effective cure. In this study, we have used molecular dynamics simulations, focusing on non-bonded interactions and thermal properties, to explore the effects of M114T mutation on PMP2 at the temperatures of 305K, 310K and 315K. Our findings indicate that the mutation slightly destabilizes PMP2, reducing its structural integrity by decreasing hydrogen bonds and altering few salt bridges, although the differences are minimal. Additionally, the mutant exhibits slightly increased thermal diffusivity. A non-linear change in C_v with temperature was also observed in both protein systems. This work further extends to verify the Maxwell-Boltzmann distribution law and demonstrate the Gaussian nature of the temperature fluctuations in the protein systems.

Keywords
Charcot-Marie-Tooth 1A, Comparative analysis, M114T mutant, NAnoscale Molecular Dynamics.

Article information
Manuscript received: September 24, 2024; Revised: January 13, 2025; Accepted: January 15, 2025
DOI https://doi.org/10.3126/bibechana.v22i1.70049

1 Introduction

Neurons are a type of specialized cells in the nervous system through which electrical impulses, also known as action potential, propagate to different cells in the rest of the body [1]. For efficient transmission of electrical impulses, the axons in the neurons are insulated by concentric layers of plasma membranes called a myelin sheath [2]. In the central nervous system, the Oligodendrocyte cells make and maintain myelin sheath, whereas in the peripheral nervous system this is done by the Schwann cells [3]. A single schwann cell forms one myelin sheath. High level of saturated long chain fatty acids is present in myelin along with Fatty acid binding proteins like Myelin Basic Protein (MBP) and Peripheral Myelin Protein 2 (PMP2) which play a crucial role in inter-molecular cohesion with the lipids which stack the myelin layers together to form myelin sheath [4,5]. In particular, PMP2 is one of the most prevalent constituents in the myelin of the human PNS [6].

Mutations in PMP2 protein have been linked with various types of Charcot-Marie-Tooth (CMT) disease [7–10], a Hereditary Motor and Sensory Neuropathy (HMSN), which primarily targets the

Peripheral Nervous System [11]. One such recently discovered mutation in this protein is M114T, which was associated with the CMT type 1A disease in German and Bulgarian families [10]. Many attempts, including using ascorbic acid [12], have failed to cure CMT disease, as no significant improvement in nerve conduction velocity was observed. To date, no therapeutic cure exists.

Research on the PMP2 protein has revealed its tetragonal crystal structure in the space group P 41 21 2. Its molecular weight is approximately 15 kDa, and has high solubility in aqueous buffer solution. The structure of protein plays an important role in proper functioning. Destabilized structures can result in the loss of function which can lead to aggregation of protein and formation of toxic species. In the case of this protein, there are ten anti-parallel β strands and two α helices [13]. There is a fatty acid, Palmitate, inside the barrel shape of the protein. From the atomistic molecular dynamics simulation study of wild-type PMP2, it was found that the absence of this fatty acid increased the dynamics in the 2α helix [14]. Non-bonded interactions within protein structures dictate their integrity and function, with alterations leading to misfolding and aggregates linked to diseases like Alzheimer's and Parkinson's.. The mutant protein has a similar tetragonal crystal structure, but with increased fatty acid binding ability. Also, using the CD spectroscopy, the melting temperature for wild-type protein was found to be $+61.6$°C whereas that for M114T mutant was $+49.2$°C [15].

Figures 1 and 2 show the chemical structures of Methionine (left) and Threonine (right) at the mutation site, and the normal PMP2 protein with Methionine and Threonine at position 114, respectively.

CMT disease has a low mortality rate, with children being at relatively higher risk than adults [16]. However, there is a greater risk on the mental health of patients as they are psychologically more vulnerable. Issues like depression, anger, guilt, and frustration due to lack of independence could disturb their mental peace and well-being [17]. While previous research has explored the structural and functional roles of PMP2, there has been limited focus on the effects of this specific mutations on interaction dynamics and thermal behavior. So, this research work got attention towards the comparative study of non-bonded interactions and thermal properties in normal and M114T mutant human PMP2 protein. Also, no such study has yet been done at temperatures of 305 K, 310 K, and 315 K – the normal and extreme core body temperatures in humans [18, 19]. As there are many enzymatic activities essential for cellular processes, studying the changes in the thermal properties and their impact on them is crucial to understanding the effects of the mutation on the body, which can aid in the development of proper therapeutic drugs.

We have presented the details regarding the methods and methodology in section 2, computational details in section 3, and the results and discussions in section 4. Finally, the conclusions and concluding remarks are presented in the section 5.

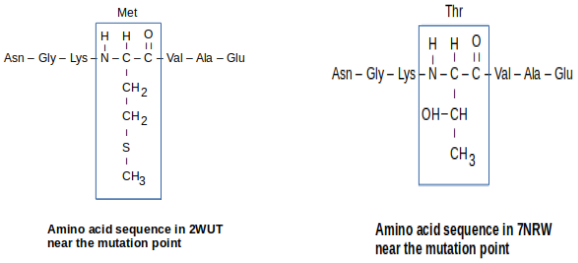

Figure 1: Chemical structure of Methionine (left) and Threonine (right) in the amino acid chain of PMP2 near mutation cite.

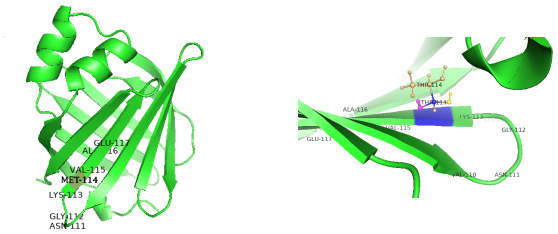

Figure 2: Normal PMP2 protein with Methionine at 114^{th} position (left), and mutant PMP2 protein with Threonine at the 114^{th} position (right).

2 Methods and Methodology

In Molecular Dynamics, different properties such as RMSD, H-bonding, Salt Bridge formation, etc can be estimated using the information of the trajectories of the particles in 6N-dimensional phase space. For this, at first the particles are assigned a position. Then, the subsequent positions during simulation are generated by solving the equation of motion given by,

$$m_i \frac{\partial^2 r_i(t)}{\partial t^2} = F_i\{r_i(t)\} - \gamma_i \frac{dr_i(t)}{dt} + R_i(t) \quad (1)$$

where $m_i \frac{\partial^2 r_i(t)}{\partial t^2}$, $F_i\{r_i(t)\}$ and $\gamma_i \frac{dr_i(t)}{dt}$ are the net force on the i^{th} atom, total force on the i^{th} atom due to the neighbouring atoms, and damping force, respectively at time t. And $R_i(t)$ accounts for the random force that acts on the atoms [20].

Both the bonded (V_B) and non-bonded (V_{NB}) potentials act on the system. If the i^{th} and j^{th} atom at distance r_{ij} have partial charges Q_i and Q_j, then the total potential (V_T) is obtained as,

$$V_T = V_B + V_{NB} \quad (2)$$

where $V_B = V_{bond} + V_{angle} + V_{improper} + V_{proper}$, and $V_{NB} = V_{LJ} + V_{coulomb}$

The Lennard-Jones potential V_{LJ}, between a pair of atoms is given by the equation [21],

$$V_{LJ} = 4\varepsilon\left[\left(\frac{\sigma}{r}\right)^{12} - \left(\frac{\sigma}{r}\right)^{6}\right] \quad (3)$$

And the Coulomb electrostatic interaction potential $V_{coulomb}$ is given by the equation,

$$V_{coulomb} = \frac{Q_i \cdot Q_j}{4\pi\epsilon_m r_{ij}} \quad (4)$$

2.1 Root Mean Square Deviation (RMSD)

The RMSD at an instant is the standard deviation of the position of the atom from mean position at that instance. It tells about the stability of the protein over time and can be used to compare the structure and conformation of two proteins. Higher value of RMSD means reduced stability. The equation that gives the RMSD of a system [22] is,

$$RMSD\left(t_i\right) = \sqrt{\left(\frac{\sum_{\alpha=1}^{N_\alpha}\left(\overrightarrow{r_\alpha}\left(t_i\right) - \langle\overrightarrow{r_\alpha}\rangle\right)^2}{N_t}\right)} \quad (5)$$

With,

$$\langle\overrightarrow{r_\alpha}\rangle = \frac{1}{N_t}\sum_{i=1}^{N_t}\langle\overrightarrow{r_\alpha}\left(t_i\right)\rangle$$

Here, N_α and N_t respectively represent the number of atoms and number of time steps over which atomic positions are being compared, $\overrightarrow{r_\alpha}\left(t_i\right)$ represents the position of atom α at time t_i and $\langle\overrightarrow{r_\alpha}\left(t_i\right)\rangle$ represents the corresponding average value [23].

2.2 Hydrogen Bonds

Hydrogen bond is a non-bonded interaction, so the bonds are not stable over time. As such, the stability and strength can be understood only by analysing the average frequency of formation of H-bonds. It contributes to the elastic stiffness of the protein and its structural stability. For moderate strength H-bonding, which is mainly electrostatic, the donor-acceptor distance is 2.5 Å - 3.2 Å [24]. In this research, cutoff distance and angle for H-bonds is taken as 3.2 Å and 30°, respectively. However, due to this approximation, the weak H-bondings will not be taken into account, which might bring some error in the observed results.

2.3 Salt Bridges

Salt bridge is a type of non-bonded interaction that exists between acidic and basic residues. If such residues are within the cutoff distance than they are counted as salt bridges. Here, the oxygen-nitrogen cutoff distance for the salt bridges is taken as 3.2 Å. Salt bridges prevent the diffusion of solution [25].

2.4 Gaussian Distribution

Gaussian distribution is one of the widely observed distribution identified by the probability distribution function [26],

$$P(x) = \frac{1}{\sqrt{2\pi}\sigma_x}\exp\left(-\frac{\left(x - \langle x\rangle\right)^2}{2\sigma_x^2}\right) \quad -\infty \le x \le +\infty \quad (6)$$

where x is the random variable, whose expectation is $\langle x\rangle$ and standard deviation is σ_x.

The temperature fluctuation of the system in the NVE ensemble is expected to follow the Gaussian distribution [22].

2.5 Maxwell-Boltzmann Distribution Law

According to Maxwell and Boltzmann [27, 28], the distribution of molecular velocity (v) of an ideal gas of molecular mass m at absolute temperature T is described by the function,

$$f(v) = \sqrt{\frac{2}{\pi}}\frac{v^2 e^{-\frac{v^2}{2a^2}}}{a^3}, \qquad v \ge 0 \quad (7)$$

With parameter $a = \sqrt{\frac{K_B T}{m}}$, where K_B is Boltzmann constant.

Using the expression for Kinetic energy,

$$E_k = \frac{1}{2}mv^2 = \frac{3}{2}K_B T$$

and with proper normalization, we get the probability distribution function for the kinetic energy [22] as,

$$f\left(E_k\right) = \frac{2}{\sqrt{\pi}}\frac{1}{\left(K_B T\right)^{\frac{2}{3}}}\sqrt{E_k}\exp\left(-\frac{E_k}{K_B T}\right) \quad (8)$$

2.6 Thermal Diffusivity

The three-dimensional heat equation is,

$$\frac{\partial T\left(\overrightarrow{r}, t\right)}{\partial t} = D \cdot \nabla^2 T\left(\overrightarrow{r}, t\right) \quad (9)$$

The time dependence of the average temperature in the water-sphere system considered here is given by the equation [22],

$$\langle T\rangle\left(t\right) = T_{bath} + 6\cdot\frac{T_{initial} - T_{bath}}{\pi^2}\sum_{n=1}^{\infty}\frac{1}{n^2}\exp\left[-\left(\frac{n\pi}{R}\right)^2 Dt\right] \quad (10)$$

where T_{bath} and $T_{initial}$ are the temperatures of outer shell of sphere and the initial temperature of the interior of sphere, respectively. R (= 25 Å) is

radius of sphere excluding the outer shell of thickness 5 Å.

To fit a curve with the obtained data, we have approximated to the first 11 terms only, and the other terms are neglected. So, the expression considered here is,

$$\langle T \rangle (t) = 200 + 66.87 \cdot \left[\sum_{i=1}^{\infty} \frac{1}{i^2} \cdot e^{-i^2 \cdot 0.0158 \cdot D \cdot t} \right] \tag{11}$$

2.7 Specific Heat Capacity at constant volume (C_v)

Molar specific heat capacity is the amount of heat required to raise the temperature of one mole of a substance by one Kelvin. In NAMD, the specific heat capacity at constant volume can be obtained from a single NVT production simulation using the equation [29, 30],

$$C_v = \frac{\langle E^2 \rangle - \langle E \rangle^2}{K_B T^2} \tag{12}$$

where $\langle E \rangle$ is the average of the total energy and $\langle E^2 \rangle$ is the average of the square of the total energy.

3 Computational details

This research is based on the theoretical and computational techniques of molecular dynamics. For this, the structure of the wild-type and M114T mutant PMP2 proteins were obtained from RCSB.org. The PDB ID of the chosen wild-type protein is 2WUT and of the chosen mutant is 7NRW. Then, the simulation is performed using the NAMD (NAno scale Molecular Dynamics) and VMD (Visual Molecular Dynamics) softwares. However, in molecular simulations using these softwares, there are some approximations like fixed force fields and cutoff distances which might not fully capture the long-range interactions.

At first, steps for the energy minimization are performed, followed by system equilibration. Finally, production simulation is run to obtain the final data. The RMSD is calculated from the equilibration output to check for the system stability before starting the production run, whereas rest of the analysis is done from the output of production run. For this, six systems are designed: two proteins, each kept at temperatures of 305 K, 310 K, and 315 K. The system's pH is set to 7.4, with a 12 Å cutoff distance, 16 Å pairlist distance, and an initial pressure of 1 bar. This limited cutoff for pairlist distance could lead to the interactions at the boundaries not being accounted, which might lead to inaccuracies in energy calculations; however, with a 2 fs timestep, these inaccuracies are expected to be minimal.. Also, for the study of non-bonded interactions, some K^+ and Cl^- are added to set the system to a 0.15 M/Litre concentration; however, for the study of thermal diffusivity, no ions are placed. The proteins are solvated with TIP3 water using modified charmm force field (CHARMM 36m). Equilibration and production both are done in the NVT ensemble. The details of the setup are as follows:

For the study of non-bonded interactions, the wild-type PMP2 (2WUT) with 2,154 atoms is placed in a cubical water box of side length 67 Å. The study is done at the three temperatures with minute difference in the total number of atoms: 28,027 atoms at 305 K, 27,972 atoms at 310 K, and 28,009 atoms at 315 K. However, in mutant protein (7NRW) with 2,151 atoms, the cubical box is of side length 65 Å. The number of atoms for mutant at 305 K is 25,711, at 310 K is 25,741, and at 315 K is 25,720. The parameters, as mentioned above, are the same at all temperatures.

Furthermore, for the study of thermal diffusivity, both the proteins are kept inside a water sphere of radius 30 Å, with wild-type protein containing 11,551 atoms and mutant containing 11,563 atoms, at temperature of 310 K. Temperature coupling feature of NAMD is used to set the interior temperature to 300 K and that of outer shell (of thickness 5 Å) to 200 K.

At last, for the verification of Maxwell-Boltzmann law, the systems are equilibrated for 100 ps in NVT ensemble at 310 K by removing the constraints — the atoms are set free to move and none of the bonds are kept rigid. The distribution is studied from the last time frame of the simulation. In addition to this, for the study of temperature fluctuation, a 1 ns production simulation is performed in NVE ensemble by turning off the thermostat and barostat.

This approach overlooks quantum effects, crucial in biological systems, making the results purely classical. Additionally, short simulation timescales limit insights into slower or large-scale dynamics.

4 Results and Discussions

In this section, we have presented the results of the various analyses performed on the two proteins in both graphical as well as tabular form. The positions of atoms at different instances were calculated using equation (1), the vdW and electrostatic interaction energies were calculated using equations (3) and (4), respectively. Equations (5), (11) and (12) were used to calculate RMSD, thermal diffusivity and specific heat capacity at constant volume, respectively. For the verification of Maxwell-Boltzmann law of distribution of kinetic energy,

equation (8) was used, whereas to study temperature fluctuation in NVE ensemble and to fit a curve, equation (6) was considered.

The RMSD of both proteins and corresponding distribution at 305 K, 310 K and 315 K are shown in Figure (3), (4) and (5), respectively. For wild-type protein, RMSD values at 305 K, 310 K and 315 K were 0.27 Å, 0.27 Å and 0.28 Å, respectively. For mutant, RMSD values at all temperatures were approximately the same at 0.28 Å. The standard deviation in the observed RMSD of both proteins at all temperatures was approximately the same with value of 0.01. The range of fluctuation of RMSD was between 0.05 Å and 0.07 Å, with 0.07 Å being for both proteins at 315 K. Increasing trend of RMSD with increase in temperature was observed.

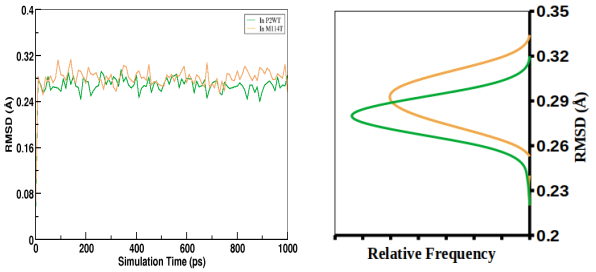

Figure 3: RMSD graph of P2WT and M114T at 305 K (left), and corresponding distribution (right)

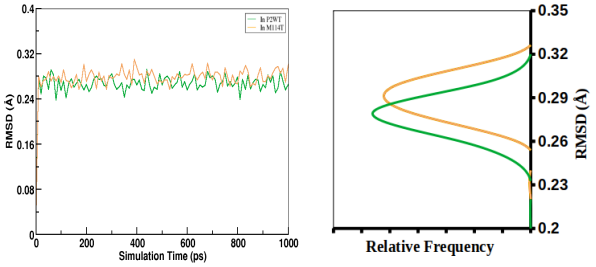

Figure 4: RRMSD graph of P2WT and M114T at 310 K (left), and corresponding distribution (right).

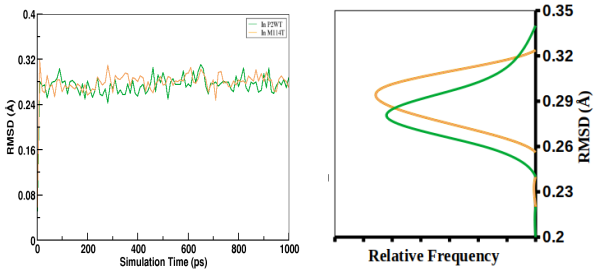

Figure 5: RMSD graph of P2WT and M114T at 315 K (left), and corresponding distribution (right).

The Number of H-bonds formed in both proteins and corresponding distribution at 305 K, 310 K and 315 K are shown in Figure (6), (7) and (8), respectively. The average number of H-bonds formed was as follows: at 305 K, 81.46 with standard deviation of 4.78 for P2WT and 79.14 with standard deviation of 4.66 for M114T; at 310 K, 80.19 with standard deviation of 4.98 for P2WT and 79.29 with standard deviation of 5.03 for M114T; at 315 K, 79.91 with standard deviation of 4.83 for P2WT and 77.28 with standard deviation of 4.97 for M114T. The fluctuation in the number of H-bonds formed was between 29 to 35. Gradual reduction in the formation of H-bonds with increase in temperature was observed. Table 1 shows the average RMSD and number of H-bonds formed in both proteins at all three temperatures.

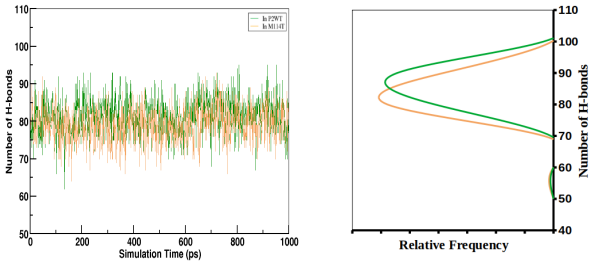

Figure 6: Graph of number of H-bonds formation over time in both proteins at 305 K (left), and corresponding distribution (right).

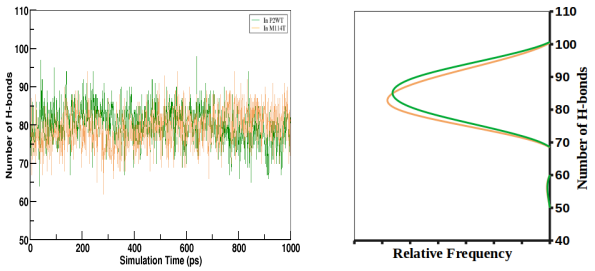

Figure 7: Graph of number of H-bonds formation over time in both proteins at 310 K (left), and corresponding distribution (right).

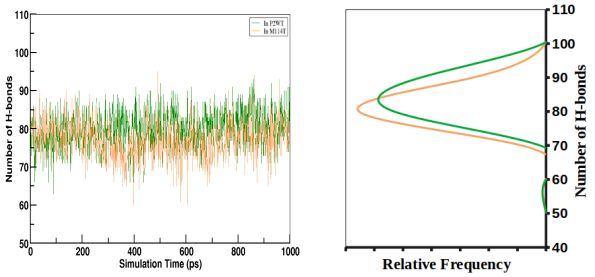

Figure 8: Graph of number of H-bonds formation over time in both proteins at 315 K (left), and corresponding distribution (right).

Table 1: For wild-type and mutant PMP2 protein at various temperatures.

Protein	**Temperature (K)**	**Avg. RMSD (Å)**	**Avg. Num of H-bonds**
P2WT (2WUT)	305	0.269	81.458
	310	0.267	80.193
	315	0.275	79.913
M114T (7NRW)	305	0.282	79.136
	310	0.279	79.288
	315	0.280	77.277

Figure (9), (10) and (11) show the bar-plot of average occupancy of salt bridges (in Å) in P2WT and M114T at 305 K, 310 K, and 315 K, respectively. Salt bridges between few residue pairs were absent, shown by vacancy in the plot; taller plots indicate weaker salt-bridges. The most noticeable difference is observed in the residue pair ASP18-LYS22 and ASP19-LYS22 at 315 K. Decreasing strength of salt-bridges with increase in temperature was observed.

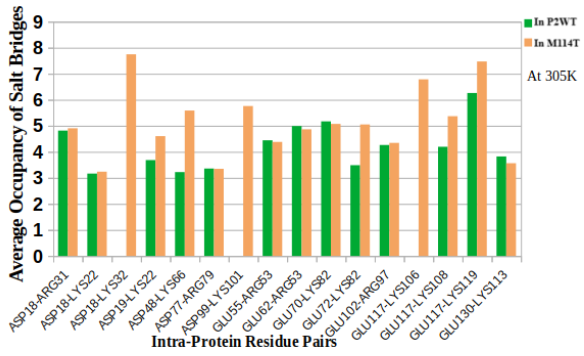

Figure 9: Average salt-bridge occupancy in both proteins at 305 K.

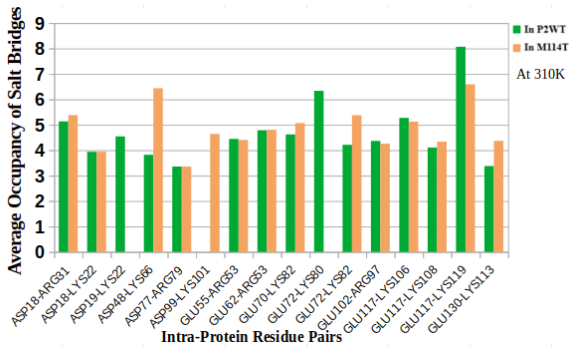

Figure 10: Average salt-bridge occupancy in both proteins at 310 K.

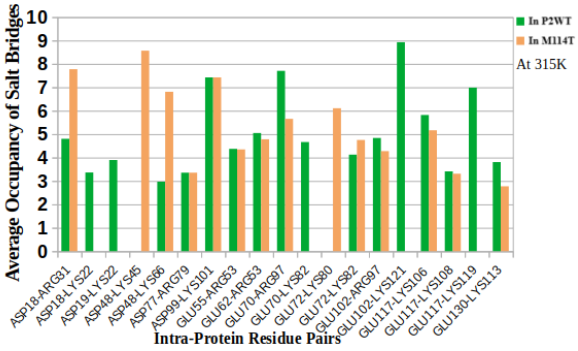

Figure 11: Average salt-bridge occupancy in both proteins at 315 K.

The particles of both systems were found to follow the Maxwell-Boltzmann law of distribution of kinetic energy. The degree of agreement of the observed data with the theoretical distribution can be seen in Figure (12). In both systems, the parameter of the observed data was about 0.61 and of the fitted curve was about 0.63. Furthermore, the graph of temperature fluctuation over time in both proteins at 310 K is shown in Figure (13) with the corresponding distribution shown in Figure (14). The observed average temperature of the system with P2WT was 308.98 K with standard deviation of 1.47, while that with M114T was 308.83 K with standard deviation of 1.53. As expected, the distribution of temperature in NVE ensemble was found to be Gaussian in nature.

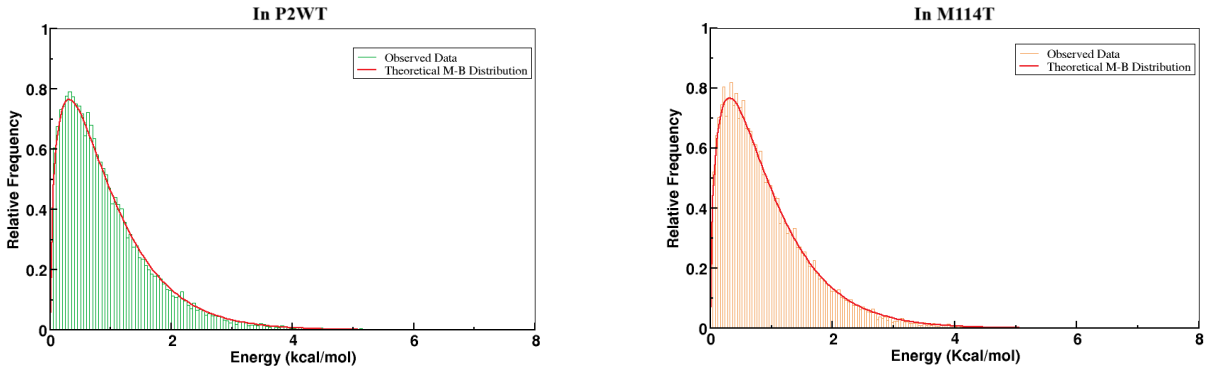

Figure 12: Maxwell-Boltzmann energy distribution at 310 K for P2WT (left), and for M114T (right).

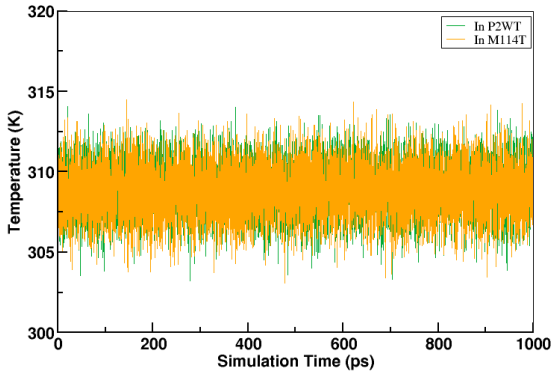

Figure 13: Graph of Temperature vs Simulation time in both proteins at 310 K.

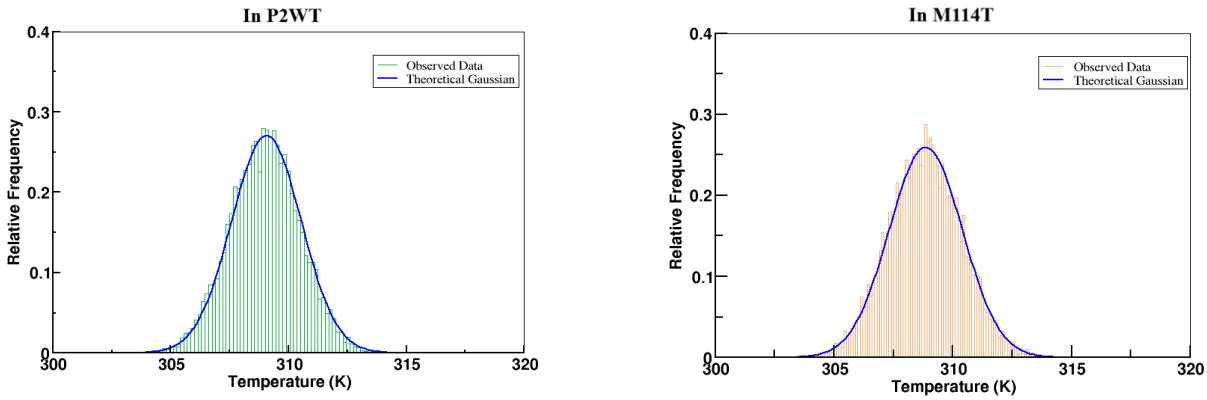

Figure 14: Temperature distribution at 310 K in P2WT (left), and for M114T (right).

Figure (15) shows the change in temperature during the course of simulation in both proteins. From the simulation, the thermal diffusivity of the P2WT was found to be $4.03\times\ 10^{-7}$ m^2s^{-1} while that for the M114T was $4.06\ \times\ 10^{-7}$ m^2s^{-1}, as show in Table 2.

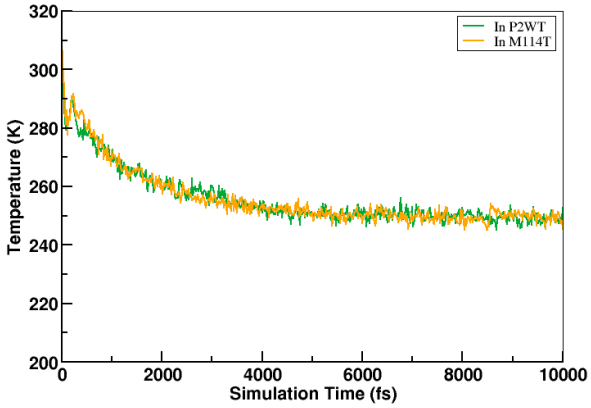

Figure 15: Graph of Temperature vs simulation time for heat diffusion in both proteins.

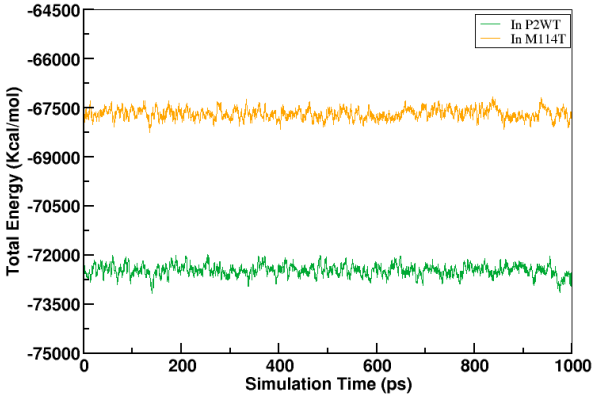

Figure 16: Graph of total energy fluctuation over time in both proteins at 305 K.

Table 2: For wild-type and mutant PMP2 protein at 310 K temperature.

Protein	**Thermal Diffusivity (m^2 s^{-1})**
P2WT (2WUT)	4.033×10^{-8}
M114T (7NRW)	4.063×10^{-8}

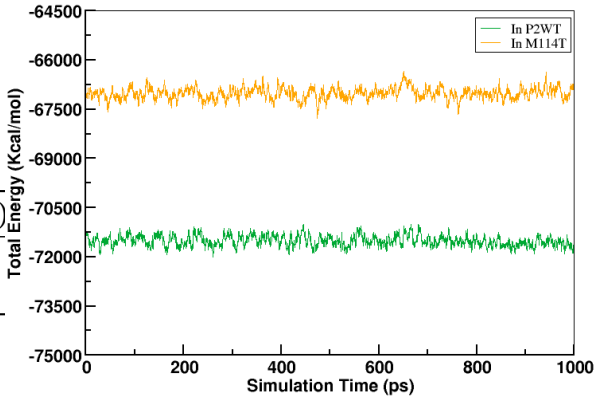

Figure 17: Graph of total energy fluctuation over time in both proteins at 310 K.

The graph of fluctuation of total energy over time in both proteins at temperature of 305 K, 310 K and 315 K are shown in Figure (16), (17) and (18), respectively. The observed specific heat capacity at constant volume for both proteins at various temperatures are shown in Table 3. At 305 K, P2WT was found to have specific heat capacity of 155.02 kcal/mol·K, which decreased to 146.45 kcal/mol·K at 310 K and increased again to 173.89 kcal/mol·K at 315 K. For M114T, at 305 K, the specific heat capacity was found to be 138.05 kcal/mol·K, which increased to 166.72 kcal/mol·K at 310 K and decreased back to 139.68 kcal/mol·K.

Table 3 also shows the observed vdW and electrostatic interaction energies along with their sum in both protein systems. These energies were found to decrease with temperature, with the P2WT system having higher energies than that of the mutant system at all temperatures.

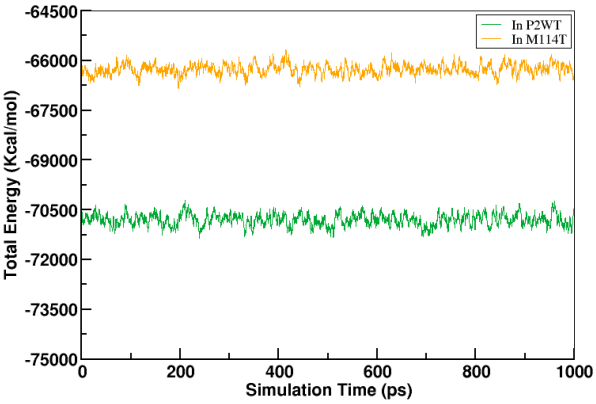

Figure 18: Graph of total energy fluctuation over time in both proteins at 315 K.

Table 3: For system with wild-type and mutant PMP2 protein at different temperatures (in kcal/mol for energies and kcal/molK for C_v).

Protein	**Temperature (K)**	**vdW**	**Electrostatic**	**Sum**	C_v **(kcal/molK)**
P2WT (2WUT)	305	8264.38	-100956.64	-92692.26	155.02
	310	8139.54	-100146.00	-92006.46	146.45
	315	8048.23	-99679.56	-91631.33	173.89
M114T (7NRW)	305	7589.58	-94075.41	-86485.83	138.05
	310	7501.03	-93641.22	-86140.19	166.72
	315	7397.91	-93043.12	-85645.21	139.68

5 Conclusion and Concluding Remarks

In this study, the RMSD of both proteins was found to be within the valid range (< 4 Å). The RMSD of wild-type protein was in the range of 0.26 Å to 0.27 Å while that of mutant was between 0.27 Å to 0.28 Å. With the increase in temperature from 305 K to 315 K, the decrease in the average number of H-bonds formation—in wild-type, from 81.46 to 79.91, whereas in mutant, from 79.14 to 77.28—suggests reduction in stability of the protein; this is due to increased thermal agitation; such a drug specimen is to be chosen that can form strong non-bonded interactions with the protein, and optimized accordingly to increase the efficiency of the treatment. A notable difference in the formation of salt-bridges were observed, especially in the residue pairs ASP18-LYS22 and ASP19-LYS22 at higher temperatures, suggesting a clear difference in diffusion of solution. The mutant showed slightly better thermal diffusivity, but compared to water, both proteins were slow at conducting heat; this is vital in understanding how heat dissipation through protein takes place during drug-protein binding. The magnitude of sum of vdW and electrostatic interaction energies is higher in the system with wild-type protein suggesting a stronger non-bonded profile compared to that with mutant; it decreases with increase in temperature in both proteins which is due to increase in mean free path of the atoms. Finally, the C_v of both systems were found to have a non-linear (concave nature) change, with system of wild-type protein being generally higher; drugs should be designed accordingly to prevent protein denaturation caused by heat generated during drug-protein binding. This unusual variation of C_v in both systems is not well understood.

We found the necessity to study the variation of C_v of both proteins at smaller temperature increments. Additionally, studying the vdW and Electrostatic interaction energies within the proteins, as well as their mechanical and other transport properties, is crucial for gaining a deeper insight into the effects of this mutation, and for the development of a therapeutic drug for CMT1A disease.

Acknowledgements

P.A. expresses deep gratitude to all the teachers of the Department of Physics, Butwal Multiple Campus for their constant support and guidance throughout this research work. He also extends his sincere thanks to his family and friends who played a pivotal role in advising and motivating him during this course.

References

[1] J. A. Kiernan and M. L. Barr. *Barr's the human nervous system: An anatomical viewpoint*. Lippincott Williams & Wilkins, 2009.

[2] J. R. Augustine. *Human neuroanatomy*. Academic Press, 2008.

[3] C. Noback, N. Strominger, R. Demarest, and D. Ruggiero. *The human nervous system: Structure and function: Sixth edition*. Springer Science & Business Media, 2005.

[4] C. Readhead, B. Popko, N. Takahashi, H. D. Shine, R. A. Saavedra, R. L. Sidman, and L. Hood. Expression of a myelin basic protein gene in transgenic shiverer mice: Correction of the dysmyelinating phenotype. *Cell*, 48(4):703–712, 1987.

[5] S. Schmitt, L. Cantuti Castelvetri, and M. Simons. Metabolism and functions of lipids in myelin. *Biochimica et Biophysica Acta (BBA) – Molecular and Cell Biology of Lipids*, 1851(8):999–1005, 2015.

[6] S. DeArmond, G. Deibler, M. Bacon, M. Kies, and L. Eng. A neurochemical and immunocytochemical study of p2 protein in human and bovine nervous systems. *Journal of Histochemistry Cytochemistry*, 28(12):1275–1285, 1980.

[7] M. Baga, S. Rizzi, C. Spagnoli, D. Frattini, F. Pisani, and C. Fusco. A novel family with demyelinating charcot–marie–tooth disease caused by a mutation in the pmp2 gene: A case series of nine patients and a brief review of the literature. *Children*, 10(5):901, 2023.

[8] A. Geroldi, V. Prada, F. Veneri, L. Trevisan, P. Origone, M. Grandis, A. Schenone, C. Gemelli, P. Lanteri, P. Fossa, et al. Early onset demyelinating charcot-marie-tooth disease caused by a novel in-frame isoleucine deletion in peripheral myelin protein 2. *Journal of the Peripheral Nervous System*, 25(2):102–106, 2020.

[9] W. W. Motley, P. Palaima, S. W. Yum, M. A. Gonzalez, F. Tao, J. V. Wanschitz, A. V. Strickland, W. N. Löscher, E. De Vriendt, S. Koppi, et al. De novo pmp2 mutations in families with type 1 charcot–marie–tooth disease. *Brain*, 139(6):1649–1656, 2016.

[10] P. Palaima, T. Chamova, S. Jander, V. Mitev, C. Van Broeckhoven, I. Tournev, K. Peeters, and A. Jordanova. Peripheral myelin protein 2–a novel cluster of mutations causing charcot-marie-tooth neuropathy. *Orphanet Journal of Rare Diseases*, 14:1–11, 2019.

[11] S. Ruskamo, T. Nieminen, C. K. Kristiansen, G. H. Vatne, A. Baumann, E. I. Hallin, A. Raasakka, P. Joensuu, U. Bergmann, I. Vattulainen, et al. Molecular mechanisms of charcot-marie-tooth neuropathy linked to mutations in human myelin protein p2. *Scientific Reports*, 7(1):6510, 2017.

[12] J. Burns, R. A. Ouvrier, E. M. Yiu, P. D. Joseph, A. J. Kornberg, M. C. Fahey, and M. M. Ryan. Ascorbic acid for charcot–marie–tooth disease type 1a in children: A randomised, double-blind, placebo-controlled, safety and efficacy trial. *The Lancet Neurology*, 8(6):537–544, 2009.

[13] V. Majava, E. Polverini, A. Mazzini, R. Nanekar, W. Knoll, J. Peters, F. Natali, P. Baumgärtel, I. Kursula, and P. Kursula. Structural and functional characterization of human peripheral nervous system myelin protein p2. *PLoS One*, 5(4):e10300, 2010.

[14] S. Ruskamo, R. P. Yadav, S. Sharma, M. Lehtimäki, S. Laulumaa, S. Aggarwal, M. Simons, J. Bürck, A. S. Ulrich, A. H. Juffer, et al. Atomic resolution view into the structure–function relationships of the human myelin peripheral membrane protein p2. *Acta Crystallographica Section D: Biological Crystallography*, 70(1):165–176, 2014.

[15] M. Uusitalo, M. B. Klenow, S. Laulumaa, M. P. Blakeley, A. C. Simonsen, S. Ruskamo, and P. Kursula. Human myelin protein p2: From crystallography to timelapse membrane imaging and neuropathy-associated variants. *The FEBS Journal*, 288(23):6716–6735, 2021.

[16] H. J. Park, Y.-C. Choi, J. W. Oh, and S.-W. Yi. Prevalence, mortality, and cause of death in charcot-marie-tooth disease in korea: a nationwide, population-based study. *Neuroepidemiology*, 54(4):313–319, 2020.

[17] A. Arnold, M. McEntagart, and D. S. Younger. Psychosocial issues that face patients with charcot-marie-tooth disease: The role of genetic counseling. *Journal of Genetic Counseling*, 14(4):307–318, 2005.

[18] W. P. Cheshire Jr. Thermoregulatory disorders and illness related to heat and cold stress. *Autonomic Neuroscience*, 196:91–104, 2016.

[19] D. F. Danzl and R. S. Pozos. Accidental hypothermia. *New England Journal of Medicine*, 331(26):1756–1760, 1994.

[20] M. P. Allen and D. J. Tildesley. *Computer simulation of liquids*. Oxford University Press, 2017.

[21] J. E. Lennard-Jones. Cohesion. *Proceedings of the Physical Society*, 43(5):461, 1931.

[22] J. C. Phillips, R. Braun, W. Wang, J. Gumbart, E. Tajkhorshid, E. Villa, C. Chipot, R. D. Skeel, L. Kale, and K. Schulten. Scalable molecular dynamics with namd. *Journal of computational chemistry*, 26(16):1781–1802, 2005.

[23] J. C. Phillips, D. J. Hardy, J. D. Maia, J. E. Stone, J. V. Ribeiro, R. C. Bernardi, R. Buch, G. Fiorin, J. Hénin, W. Jiang, et al. Scalable molecular dynamics on cpu and gpu architectures with namd. *The Journal of Chemical Physics*, 153(4), 2020.

[24] G. Jeffrey. *An introduction to hydrogen bonding*. Oxford University Press, 1997.

[25] Y. Marcus and G. Hefter. Ion pairing. *Chemical Reviews*, 106(11):4585–4621, 2006.

[26] X. Zhang. Gaussian distribution. In *Encyclopedia of machine learning and data mining*, pages 1–5. 2010.

[27] L. Boltzmann. Weitere studien über das wärmegleichgewicht unter gasmolekülen. In *Kinetische Theorie II*, pages 115–225. 1970.

[28] J. Maxwell. Illustrations of the dynamical theory of gases. *Philosophical Magazine*, 19:19–32, 1867.

[29] K. Huang. *Statistical mechanics*. John Wiley & Sons, 2008.

[30] J. Powrel and N. P. Adhikari. Thermal properties of normal and sickled hemoglobin protein. *BIBECHANA*, 18(1):140–148, 2021.